Published June 30, 2014

Determinants of ligand selectivity in a cyclic nucleotide–regulated potassium channel

João Pessoa,[1,2] Fátima Fonseca,[1] Simone Furini,[3] and João H. Morais-Cabral[1]

[1]Instituto de Biologia Molecular e Celular and [2]Instituto de Ciências Biomédicas Abel Salazar, Universidade do Porto, 4150-180 Porto, Portugal

[3]Department of Medical Biotechnologies, University of Siena, 53100 Siena, Italy

Cyclic nucleotide–binding (CNB) domains regulate the activity of channels, kinases, exchange factors, and transcription factors. These proteins are highly variable in their ligand selectivity; some are highly selective for either cAMP or cGMP, whereas others are not. Several molecular determinants of ligand selectivity in CNB domains have been defined, but these do not provide a complete view of the selectivity mechanism. We performed a thorough analysis of the ligand-binding properties of mutants of the CNB domain from the MlotiK1 potassium channel. In particular, we defined which residues specifically favor cGMP or cAMP. Inversion of ligand selectivity, from favoring cAMP to favoring cGMP, was only achieved through a combination of three mutations in the ligand-binding pocket. We determined the x-ray structure of the triple mutant bound to cGMP and performed molecular dynamics simulations and a biochemical analysis of the effect of the mutations. We concluded that the increase in cGMP affinity and selectivity does not result simply from direct interactions between the nucleotide base and the amino acids introduced in the ligand-binding pocket residues. Rather, tighter cGMP binding over cAMP results from the polar chemical character of the mutations, from greater accessibility of water molecules to the ligand in the bound state, and from an increase in the structural flexibility of the mutated binding pocket.

INTRODUCTION

The cyclic nucleotides cAMP and cGMP are important secondary messengers in several signal transduction pathways, including those of vision and olfaction (Zhang and Cote, 2005; Rehmann et al., 2007; Pifferi et al., 2010). Action of these small molecules is, in many cases, dependent on binding to a cyclic nucleotide–binding (CNB) domain. Ligand binding induces a conformational change in the CNB domain, which is propagated to an effector domain leading to a functional alteration (Rehmann et al., 2007). Among the proteins with cyclic nucleotide–dependent activity, there are three families of cation tetrameric channels (Fig. S1): the eukaryotic CNG channels (Craven and Zagotta, 2006); the eukaryotic hyperpolarization-activated CNG (HCN) channels (Craven and Zagotta, 2006); and the bacterial cyclic nucleotide–regulated channels, which include the MlotiK1 potassium channel (Clayton et al., 2004; Nimigean et al., 2004). All of these channels have subunits with six transmembrane helices and a C-terminal cytoplasmic CNB domain.

The ligand-binding pocket in CNB domains (Fig. 1 A) has a shallow cavity, formed by residues from several structural motifs (the β4–β5 hairpin, the αP helix, and loop of the phosphate-binding cassette [PBC]) and a lid that closes over the nucleotide (Rehmann et al., 2007). In MlotiK1, the lid is formed by the C-terminal αC helix and includes an arginine (R348) that interacts directly with the nucleotide base (Clayton et al., 2004). Strikingly, cyclic nucleotide selectivity varies greatly among proteins with CNB domains, with some proteins strongly favoring cAMP while others favor cGMP. For example, the bovine rod photoreceptor and olfactory CNG channels are ∼40 times more sensitive to cGMP than to cAMP, as measured from the ratio of the $K_{1/2}$ for channel activation (Altenhofen et al., 1991). In the olfactory channel, mutation of a threonine at the C-terminal end of the PBC to alanine was sufficient to invert selectivity from a 40-fold preference for cGMP to a 3.3-fold preference for cAMP. However, the equivalent mutation in the rod photoreceptor channel, although reducing affinity for cGMP, did not invert selectivity. However, mutation of an aspartate present in the αC helix of the bovine rod CNG channel to a non-negatively charged residue resulted in the inversion of the efficacy of cGMP versus cAMP to act as agonists (Varnum et al., 1995). Nimigean and Pagel (2007) analyzed the effect of equivalent mutations in the MlotiK1 channel. They found that mutations S308V, equivalent to the threonine in the PBC, and A352D, equivalent to the aspartate in αC helix,

Correspondence to João H. Morais-Cabral: jcabral@ibmc.up.pt

Abbreviations used in this paper: CNB, cyclic nucleotide–binding; HCN, hyperpolarization-activated CNG; MD, molecular dynamics; PBC, phosphate-binding cassette; RMSD, root-mean-square deviation.

The Rockefeller University Press $30.00
J. Gen. Physiol. Vol. 144 No. 1 41–54
www.jgp.org/cgi/doi/10.1085/jgp.201311145

Supplemental Material can be found at:
http://jgp.rupress.org/content/suppl/2014/06/26/jgp.201311145.DC1.html

Published June 30, 2014

altered the affinity for cAMP and cGMP, as predicted previously. However, these changes were relatively small, and channel ligand selectivity was not inverted. The inability to define general rules that explain selectivity in CNB domains (Cukkemane et al., 2011) is a reflection of our incomplete understanding of this mechanism, and it probably results from several factors: the difficulty of many studies to distinguish the impact of mutated residues on functional selectivity versus binding selectivity, the lack of structural analysis to complement the biochemical or functional studies, and the inexhaustive exploration of all the residues in the binding pocket of CNB domains.

The MlotiK1 channel is particularly amenable for defining the determinants of cyclic nucleotide selectivity. This channel has been well characterized at a structural, functional, and biochemical level (Clayton et al., 2004, 2008; Nimigean et al., 2004; Chiu et al., 2007; Cukkemane et al., 2007; Nimigean and Pagel, 2007; Altieri et al., 2008; Schünke et al., 2009, 2011; Peuker et al., 2013), and, by studying the isolated CNB domain, it is possible to separate ligand binding from, at least, the final steps of the mechanism of channel activation. We performed an extensive mutagenesis analysis of the residues involved in the structural interaction with the nucleotide base and evaluated the impact of these mutations on the binding of cAMP and cGMP. Ligand-binding selectivity was inverted only after three different mutations were combined; a structural analysis of this triple mutant reveals how these mutations alter the molecular details of the nucleotide-binding pocket.

MATERIALS AND METHODS

Preparation of CNB domain without ligand

MlotiK1 CNB domain mutants were expressed and purified as described previously (Clayton et al., 2004). PBS buffer containing 2 mM DTT (purification buffer) was used throughout purification. Size-exclusion chromatography was performed in a Superdex 75 column (GE Healthcare). For preparation of apo-domain, freshly purified protein was incubated overnight with cAMP agarose beads (Sigma-Aldrich), and bound protein was extensively washed with purification buffer. cAMP-free protein was eluted by unfolding with purification buffer that included 3 M guanidinium chloride (unfolding buffer). cAMP removal was monitored by determining the OD_{260}/OD_{280} ratio, as described previously (Peuker et al., 2013). Typical values varied between 0.65 and 0.90 for nucleotide-free CNB domain. Protein was first diluted to 0.3 mg/ml with unfolding buffer and then diluted threefold into refolding buffer (100 mM NaCl, 10 mM sodium phosphate, pH 7.0, 5 mM glutathione [reduced], 0.5 mM glutathione [oxidized], 0.5 mM L-arginine, and 10 mM EDTA) (Cukkemane et al., 2007) to a final concentration of 0.1 mg/ml protein and 1 M guanidinium chloride. This solution was gently stirred at 4°C for 3 h, and then the protein was concentrated to ∼0.3 mg/ml. The refolded protein was further dialyzed against refolding buffer to lower guanidinium chloride concentration to ∼50 mM. Dialyzed protein was concentrated and loaded onto a Superdex 75 size-exclusion column to remove misfolded protein (Peuker et al., 2013) (folded protein elutes at 12.0–12.5 ml, and misfolded protein elutes at 16.0–17.0 ml). Finally, refolded apo-protein was dialyzed against 10 mM HEPES buffer, pH 7.5, and 100 mM NaCl before binding assays.

Cyclic nucleotide–binding assays

Dissociation constants were determined at room temperature in 10 mM HEPES, pH 7.5, and 100 mM NaCl, with a fluorescence assay that uses the fluorescent nucleotide analogue 8-NBD cAMP (Biolog) (Cukkemane et al., 2007; Altieri et al., 2008). Cyclic nucleotides (cAMP and cGMP [both from Sigma-Aldrich], cIMP [Sigma-Aldrich], and cCMP [Biolog]) were purchased as acids or as sodium salts. For each mutant, the K_d of the fluorescent analogue was determined by titrating 50 nM 8-NBD cAMP with increasing protein concentrations and collecting fluorescence emission spectra (excitation at 471 nm) in a spectrofluorometer (Fluoromax-4; Horiba Scientific). For each protein concentration tested, emission at 536 nm was normalized as described previously (Altieri et al., 2008), and data were fitted with the following equation:

$$y = \frac{1}{1 + \frac{2}{-1 - \frac{L}{K} + \frac{P}{K} + \sqrt{\left(1 + \frac{L}{K} - \frac{P}{K}\right)^2 + 4 \times \frac{P}{K}}}},$$

where y is the normalized fluorescence intensity, K is the dissociation constant of 8-NBD cAMP, P is protein concentration, and L is 8-NBD cAMP concentration.

For determination of the dissociation equilibrium constants of cAMP or cGMP, the above assay was repeated in the presence of a competing fixed concentration of cAMP or cGMP in each sample. For determination of the competing concentration, the protein concentration that resulted in 70–80% of the maximum signal was selected and titrated with increased ligand concentrations. The ligand concentration that decreased the signal to 40–50% was then chosen for the competition assay. Data were fitted with the following equation:

$$y = G \times L1 \times \frac{2\sqrt{a^2 - 3b}\cos\left(\frac{c}{3}\right) - a}{3K1 + 2\sqrt{a^2 - 3b}\cos\left(\frac{c}{3}\right) - a} + y0,$$

where,

$$a = K1 + K2 + L1 + L2 - P$$
$$b = K2(L1 - P) + K1(L2 - P) + K1K2$$
$$c = \arccos\frac{-2a^3 + 9ab + 27K1K2P}{2\sqrt{(a^2 - 3b)^3}},$$

where y is the fluorescence intensity, $K1$ is the dissociation constant of 8-NBD cAMP, $K2$ is the dissociation constant of cAMP or cGMP, $L1$ is the 8-NBD cAMP concentration, P is total protein concentration, $L2$ is total concentration of cAMP or cGMP, G is signal gain, and $y0$ is signal offset.

For mutants displaying 8-NBD cAMP dissociation constants higher than 5 µM, a modified assay was used (Altieri et al., 2008). The concentrations of the protein and 8-NBD cAMP were fixed at approximately the K_d value and two times the K_d value, respectively, and titrated with increasing cAMP or cGMP concentrations. Data were fitted with the previous equation but with a varying cyclic nucleotide concentration.

Published June 30, 2014

Expression and purification of full-length MlotiK1 channel

Full-length MlotiK1 T284S/V288S/A352D was expressed, purified, and reconstituted as described previously for the wild-type channel (Clayton et al., 2004; Nimigean et al., 2004). In brief, MlotiK1 expressed in C41 (DE3) cells was extracted at 4°C for 30 min with PBS buffer, pH 7.4, containing 50 mM *n*-decyl-β-D-maltopyranoside (DM; Anatrace), 200 µM cAMP, 5 mM β-mercaptethanol. During purification and until gel filtration, the same buffer was used, but cAMP was excluded and the DM concentration decreased to 5 mM, unless stated otherwise. Detergent-extracted proteins were incubated with nickel beads and first washed with 50 mM imidazole to remove nonspecifically bound proteins, followed by a 200-ml wash in 2 mM DM. This ensured that cAMP bound to the triple mutant channel, which has micromolar affinity for cAMP, would dissociate from the protein. MlotiK1 was eluted in 500 mM imidazole and further purified by gel filtration on a Superdex 200 column (GE Healthcare) equilibrated in 20 mM Tris-HCl, pH 7.5, 150 mM KCl, 5 mM DM, and 3 mM DTT. Protein was immediately reconstituted in the presence of different ligand concentrations.

Liposome reconstitution and radioactive uptake assay

Proteoliposome preparation followed previously described procedures (Clayton et al., 2004; Nimigean et al., 2004; Altieri et al., 2008). In brief, 7.5 µg MlotiK1 protein was mixed with 1.5 mg *Escherichia coli* polar lipids (Avanti Polar Lipids, Inc.) in 10 mM HEPES, 5 mM *N*-methyl-β-D-glucamine (NMG), pH 7.6, and 150 mM KCl for a total volume of 150 µl. The detergent was removed by hydrophobic adsorption using Bio-Beads SM-2 (Bio-Rad Laboratories). Samples were gently stirred for 1 h at room temperature at a Bio-Beads/detergent (wt/wt) ratio of 10-15. This step was repeated twice and followed by an overnight incubation at 4°C with at a Bio-Beads/detergent (wt/wt) ratio of 20-30. Proteoliposomes were not frozen at any stage. A potassium concentration gradient was established by exchanging the external buffer to 10 mM HEPES, 5 mM NMG, pH 7.6, 20 µM KCl, and 150 mM sorbitol (sorbitol buffer) in the presence of the appropriate cAMP or cGMP concentrations, using spin columns. Uptake assays (Nimigean, 2006) were started by mixing one third of the final reaction volume of buffer-exchanged proteoliposomes with two thirds of sorbitol buffer containing 5 cps/µl $^{86}Rb^{+}$ (PerkinElmer) and the appropriate ligand concentration. Uptake was monitored after 90 min in 100-µl aliquots and normalized as described previously (Nimigean, 2006).

Purification and crystallization of T284S/V288S/A352D mutant CNB domain

Expression and purification of T284S/V288S/A352D CNB domain was performed as described previously for the wild-type domain (Clayton et al., 2004). For nucleotide removal, the protein bound to GST beads was washed with 200 ml buffer (PBS buffer containing 3 mM DTT) before incubation with thrombin. Size-exclusion chromatography was performed on a Superdex 75 column equilibrated in 10 mM Tris, pH 7.0, 100 mM NaCl, and 4 mM DTT.

Crystals of T284S/V288S/A352D mutant domain were grown using the vapor diffusion method in 24-well hanging-drop trays with a 500-µl reservoir solution of 0.15 M sodium citrate, pH 5.6, 0.9 M ammonium sulfate, and 100 mM lithium sulfate. Protein at 10 mg/ml was combined with cGMP (final concentration of 1.5 mM) and mixed with the reservoir solution at a 1:1 ratio for a final drop volume of 4 µl. Crystals appeared within 10 d at 25°C. Crystals were cryoprotected in well solution supplemented with 25% glycerol and 1.5 mM cGMP before flash cooling in liquid nitrogen. Diffraction data were collected at 100 K at the beamline 14-4 of the European Synchrotron Radiation Facility (ESRF) and processed with XDS (Kabsch, 2010) and SCALA (Evans, 2006). Mutant CNB domain crystals grew in space group $P2_12_12_1$ with two molecules in the asymmetric unit. The structure of the mutant CNB domain–cGMP complex was solved by molecular replacement with Phaser (McCoy et al., 2007) using chain A of the cGMP-bound structure (Protein Data Bank accession no. 3CL1) (Altieri et al., 2008) as the search model. Model building and refinement were performed with Coot (Emsley et al., 2010) and Phenix (Afonine et al., 2012), respectively. Ligand restraints were generated using Phenix. Figures were generated using PyMOL software (Schrödinger, LLC).

Molecular dynamics (MD) simulations

Two models were defined as corresponding to the CNB domain of wild-type MlotiK1 and of the T284S/V288S/A352D mutant, respectively. The atomic coordinates of the wild-type domain were taken from the Protein Data Bank (accession no. 3CL1) (Altieri et al., 2008). Residues 350–354 are missing in 3CL1, whereas their structure was solved in the mutant. Because these residues are close to the nucleotide-binding site, we decided to include them in both models. The initial structure of residues 350–354 in the wild-type domain was defined as an elongation of the αC helix. The final models included residues 320–354 for the wild-type CNB domain and residues 314–355 for the T284S/V288/A352 mutant domain. N and C terminals were acetylated and amidated. The default protonation state was assumed for all the ionizable residues, and histidine residues were protonated at the epsilon position. All of the water molecules that are present in the crystallographic structures were retained. The systems were solvated by ∼6,000 water molecules, and the necessary number of chloride ions was added to guarantee electrical neutrality. The atomic models were first equilibrated in the NVT ensemble (600 ps), with harmonic restraints applied to all of the heavy atoms of the protein, of cGMP, and of the crystallographic water molecules. The harmonic restraints were gradually removed in the course of 10-ns equilibration trajectories in the NPT ensemble. Production trajectories of 100 ns followed.

MD trajectories were simulated using NAMD version 2.9 (Phillips et al., 2005), with the CHARMM27 force field with CMAP corrections (MacKerell et al., 1998), and the TIP3P model for water molecules (Jorgensen et al., 1983). Pressure was kept at 1 atm by the Nosé–Hoover Langevin piston method (Martyna et al., 1994; Feller et al., 1995), with a damping time constant of 50 fs and a period of 100 fs. Temperature was kept at 300 K by coupling the system to a Langevin thermostat, with a damping coefficient of 5 ps^{-1} (Feller et al., 1995). Electrostatic interactions were treated by the particle mesh Ewald algorithm, with a grid spacing below 1 Å (Essmann et al., 1995). Van der Waals interactions were truncated at 12 Å and smoothed at 10 Å. Hydrogen atoms were restrained by the SETTLE algorithm (Miyamoto and Kollman, 1992). A time step of 2 fs was adopted to integrate the equations of motion.

Energy calculations

The energy of binding, ΔG, is defined as:

$$\Delta G = G_{complex} - G_{protein} - G_{cGMP},$$

where $G_{complex}$, $G_{protein}$, and G_{cGMP} are the energies of the complex, the isolated protein, and the nucleic acid, respectively. These energies were estimated with the MM-PBSA approach, using the single-trajectory paradigm; i.e., the structures of complex, protein, and nucleic acid were taken from the same MD trajectory. As a general rule, the single-trajectory paradigm provides accurate energy estimates only if the ligands and the protein do not change structure upon binding. However, in this study, we are interested only in energetic differences between the wild-type and the triple mutant, and not in the absolute value of the binding energies. Therefore, a less stringent condition applies to MM-PBSA calculations with the single-trajectory paradigm. Even if the structure of

Published June 30, 2014

the protein or of the ligand changes upon binding, the estimated difference in binding energy between the wild type and the mutant is still accurate, provided that these structural changes have similar energetic effects in the two systems.

The free energy of each species was calculated as:

$$G = E_{VDW} + G_{SA} + E_{COUL} + G_{PB},$$

where E_{VDW} is the Van der Waals energy, E_{COUL} is the coulombic energy, and G_{PB} and G_{SA} are polar and apolar contributions to the solvation energy. The apolar contribution to the binding energy is given by the sum of E_{VDW} and G_{SA}, whereas the sum of E_{COUL} and G_{PB} defines the polar component of the binding energy. Solvation energies were calculated with the APBS software (Baker et al., 2001). The probe radius for the definition of the molecular surfaces was 1.4 Å. The relative dielectric constants were 80 and 2, respectively, for solvent and solutes. The apolar solvation energy was assumed proportional to the solvent-accessible surface area, with proportionality constant equal to 0.0072 kcal mol^{-1} $Å^{-2}$. Binding energies were calculated as average values over the 100-ns MD trajectories. The time series of the various energy terms was tested for the presence of correlation with the Ljung–Box lack of correlation statistical test with a confidence level of 95%, as described in Furini et al. (2013). A sampling period for the MD trajectories equal to 1 ns guaranteed lack of correlation among samples in the time series of all the energy terms. This lack of correlation is necessary for defining a safe (over) estimation of the standard error affecting the calculated binding energies.

Accession numbers

The coordinates and structure factors of the mutant CNB domain–cGMP complex from the MlotiK1 channel were deposited at the Protein Data Bank under the accession number 4MUV.

Online supplemental material

Table S1 shows statistics of crystallographic data and refinement. Fig. S1 shows the sequence alignment of CNB domains from the MlotiK1, HCN2, and CNGA-1 channels, and the CNB β domain from the cGMP-dependent kinase I and CNB homology domains from the ELK and EAG1 channels. Figs. S2 and S3 illustrate two stereo views of the ligand-binding pocket of the triple mutant CNB domain from the MlotiK1 channel. Fig. S4 shows a mutant cycle analysis of mutations V288S and A352D. Fig. S5 shows representations of the ligand-binding pocket in the structure of the cGMP-bound CNB β domain from the cGMP-dependent protein kinase I. The online supplemental material is available at http://www.jgp.org/cgi/content/full/jgp.201311145/DC1.

RESULTS

Inverting ligand selectivity in the MlotiK1 channel

We determined the constants of dissociation of cAMP and cGMP for the MlotiK1 channel CNB domain (K_d: 148 ± 22 nM, $n = 6$, for cAMP; 1,731 ± 264 nM, $n = 6$, for cGMP) (Fig. 1, B–D, and Table 1); these values are

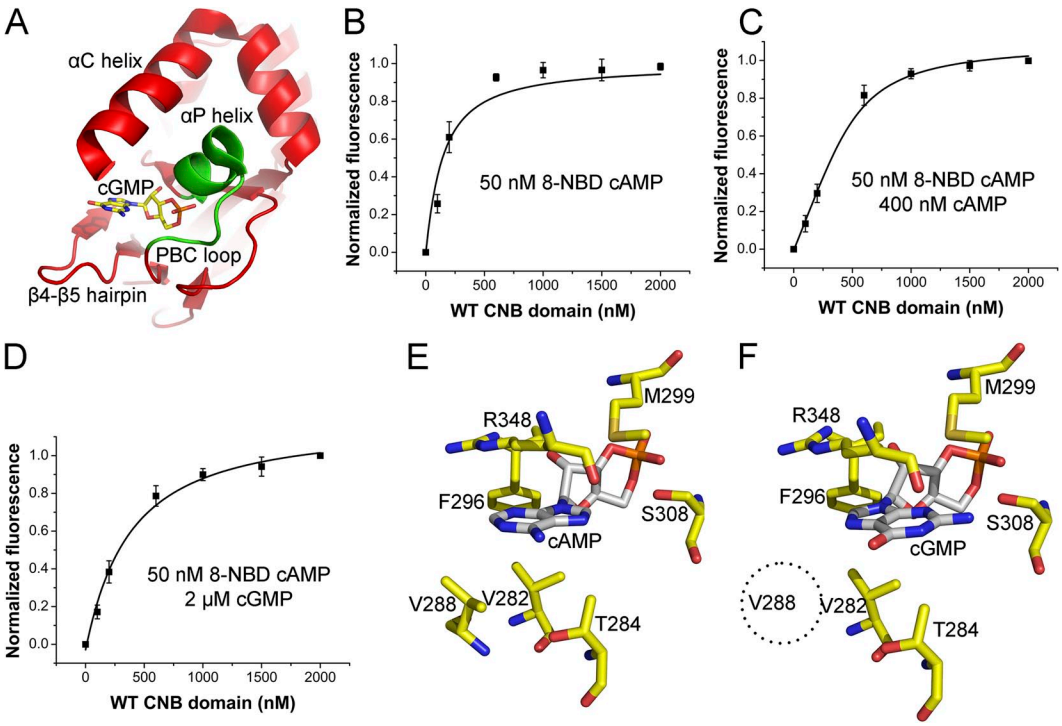

Figure 1. Cyclic nucleotide binding in the MlotiK1 CNB domain. (A) View of the CNB domain bound to cGMP. Structural elements (in red and green) that form the ligand-binding pocket are indicated. cGMP is shown as stick. (B–D) Fluorescence binding curves of the CNB domain protein titrated against 50 nM 8-NBD cAMP, (B) in the absence of competitor, and in the presence of (C) 400 nM cAMP or (D) 2 µM cGMP. K_d values determined were 171 ± 20 nM for 8-NBD cAMP, 148 ± 22 nM for cAMP, and 1,731 ± 264 nM for cGMP. Error bars indicate standard deviation of error. Experiments involve six replicates from two different protein batches. (E and F) View of residues interacting directly with ligand bases in the wild-type MlotiK1 CNB crystal structures bound to (E) cAMP (Protein Data Bank accession no. 1VP6) and (F) cGMP (Protein Data Bank accession no. 3CL1). Dotted circle indicates that V288 is one of the residues not interacting with cGMP.

Published June 30, 2014

TABLE 1

cAMP and cGMP K_ds for the wild-type and CNB domain mutants

Structural motif	Mutant	cAMP K_d	cGMP K_d	K_d ratio	*n*
		nM	*nM*		
	Wild type	148 ± 22	1,731 ± 264	11.7	6
β4–β5 hairpin	V282L	1,008 ± 53	8,951 ± 743	8.9	3
	T284N	342 ± 41	6,556 ± 633	19.2	3
	T284Q	731 ± 90	6,952 ± 1312	9.5	3
	T284S	464 ± 58	2,984 ± 379	6.4	6
	V288A	393 ± 50	2,544 ± 355	6.5	3
	V288L	201 ± 19	996 ± 163	5.2	3
	V288I	138 ± 39	797 ± 118	5.8	6
	V288S	1,205 ± 160	2,105 ± 128	1.7	4
αP helix	M299C	501 ± 99	2,942 ± 357	5.9	3
	M299Q	734 ± 134	11,649 ± 2,621	15.9	3
C terminus	A352S	174 ± 23	727 ± 160	4.2	3
	A352D	256 ± 29	850 ± 121	3.3	6
αC helix	R348A	24,822 ± 3182[a]	38,781 ± 2,449[a]	1.6	3
	R348N	19,142 ± 507[a]	32,106 ± 3,844[a]	1.7	3
	R348Q	25,097 ± 2,216[a]	46,062 ± 5,609[a]	1.8	3
	R348K	16,446 ± 842[a]	23,547 ± 982[a]	1.4	3
	R348Y	24,174 ± 2,214[a]	33,172 ± 4,771[a]	1.4	3
V288S/A352S		691 ± 72	749 ± 75	1.1	3
V288S/A352D		547 ± 111	351 ± 95	0.64	3
T284S/V288S/A352D		2,190 ± 347	336 ± 126	0.15	6

K_ds were determined by competition at a constant ligand concentration and with variable protein concentration; except for those marked with footnote a. K_d ratio is calculated from (cGMP K_d/cAMP K_d); *n*, number of repetitions.

[a]K_ds were determined by competition at a constant protein concentration and with variable ligand concentration.

larger than the values reported by others (Cukkemane et al., 2007), but the discrepancy does not alter the conclusions of our study, as we are interested in understanding the molecular basis of the relative preference of one nucleotide over the other, and we have used the same procedure throughout this study (exceptions are noted). Our measurements show that the domain is 12 times more selective for cAMP than for cGMP, as defined from the ratio of the experimentally determined affinities for the two ligands. This nucleotide preference is also reflected in the nucleotide concentration dependence of channel activity measured using an

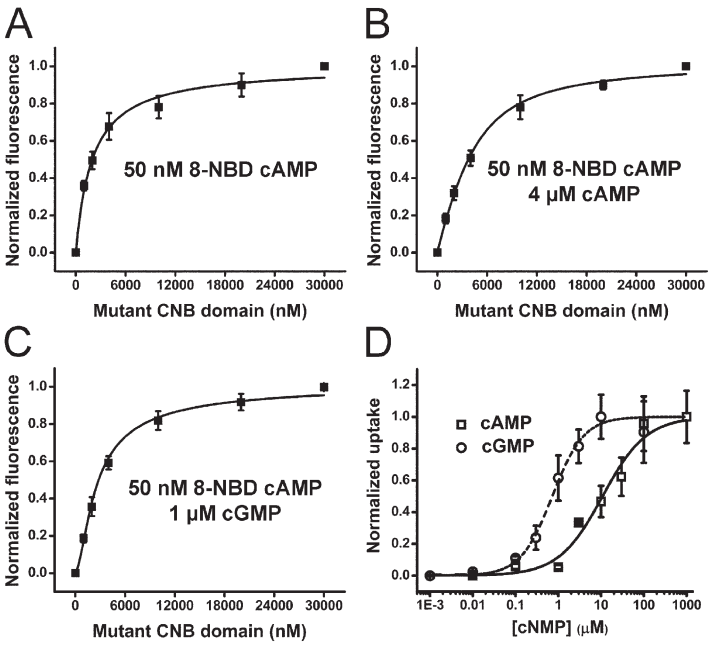

Figure 2. Titration experiments with the MlotiK1 T284S/V288S/A352D mutant. (A–C) Fluorescence binding curves of triple mutant CNB domain titrated against 50 nM 8-NBD cAMP, (A) in the absence of competitor and in the presence of (B) 4 µM cAMP or (C) 1 µM cGMP. The K_d values determined were 2,005 ± 160 nM for 8-NBD cAMP, 2,190 ± 347 nM for cAMP, and 336 ± 126 nM for cGMP. (D) Functional analysis of the T284S/V288S/A352D MlotiK1 potassium channel using an $^{86}Rb^+$ uptake assay. Normalized uptake by channel reconstituted in liposomes as a function of ligand concentration (circles, cGMP; squares, cAMP) was fitted with a Hill equation (cGMP: $K_{1/2}$ = 0.6 ± 0.1 µM and Hill coefficient = 1.3; cAMP: $K_{1/2}$ = 7.4 ± 3.3 µM and Hill coefficient = 0.84). Error bars indicate standard deviation of error. Data in fluorescence binding assays involved six replicates from two different protein batches. Radioactivity uptake assay involved three to eight replicates from three different protein batches.

Published June 30, 2014

$^{86}Rb^{+}$ flux assay; the channel has a higher sensitivity for cAMP ($K_{1/2}$ values of 110 ± 20 nM) than for cGMP (920 ± 110 nM) (Altieri et al., 2008).

A comparison of the MlotiK1 CNB domain structures bound to cAMP and cGMP (Fig. 1, E and F) shows that the residues that are within 4 Å of the nucleotide bases and which probably determine much of the binding properties of the domain are: V282 and T284 in the β4–β5 hairpin; F296, M299, and S308 in different sections of the PBC; and R348 in the αC helix, the lid of the binding pocket. The most obvious difference in the interactions established by cAMP and cGMP is V288. This residue is positioned in the β4–β5 hairpin and is within interacting distance of the cAMP base but not of cGMP (Fig. 1, E and F). Confirming the importance of these local interactions for the ligand-binding properties of the domain, we inverted ligand selectivity in the MlotiK1 CNB domain through a combination of mutations at three of these residues (T284S/V288S/A352D). This mutant domain shows a 6.5× preference for cGMP or, to allow a direct comparison with the wild-type value, a 0.15× preference for cAMP. Relative to the wild-type domain, these mutations decreased cAMP affinity (K_d cAMP: 2,190 ± 347 nM) and increased cGMP affinity (K_d cGMP: 336 ± 126 nM) (Fig. 2, A–C, and Table 1).

Reflecting the ligand-binding properties of the isolated mutant domain, the $K_{1/2}$ values for the concentration dependence of activity in the triple mutant channel show a functional preference for cGMP over cAMP ($K_{1/2}$ of ∼600 nM for cGMP and ∼7 µM for cAMP) (Fig. 2 D). Ligand efficacy in the wild-type and triple mutant channels was estimated by measuring the $^{86}Rb^{+}$ flux after 90 min in the presence of saturating concentrations of ligand (>100 times higher than the $K_{1/2}$). The maximum normalized flux for the wild-type channel is 0.29 ± 0.11 (n = 7) for cAMP and 0.18 ± 0.07 (n = 6) for cGMP. For the mutant, the values are 0.39 ± 0.07 (n = 6) for cAMP and 0.33 ± 0.05 (n = 6) for cGMP. Because of the limitations inherent to the assay, these values have to be considered carefully, but they show that unlike for ligand sensitivity, the three mutations do not appear to greatly alter the functional efficacy of the ligands.

Structure of the triple mutant

We determined the x-ray structure of the T284S/V288S/A352D mutant domain in complex with cGMP at 1.25 Å (Figs. 3, S2, and S3, and Table S1). These crystals contain two protein copies in the asymmetric unit, which are for the most part indistinguishable.

A comparison of the triple mutant structure to the wild-type domain structure in complex with cGMP (Protein Data Bank accession no. 3CL1) (Altieri et al., 2008) reveals high overall structural similarity (Fig. 3 A), with a backbone root-mean-square deviation (RMSD) of 0.60 Å.

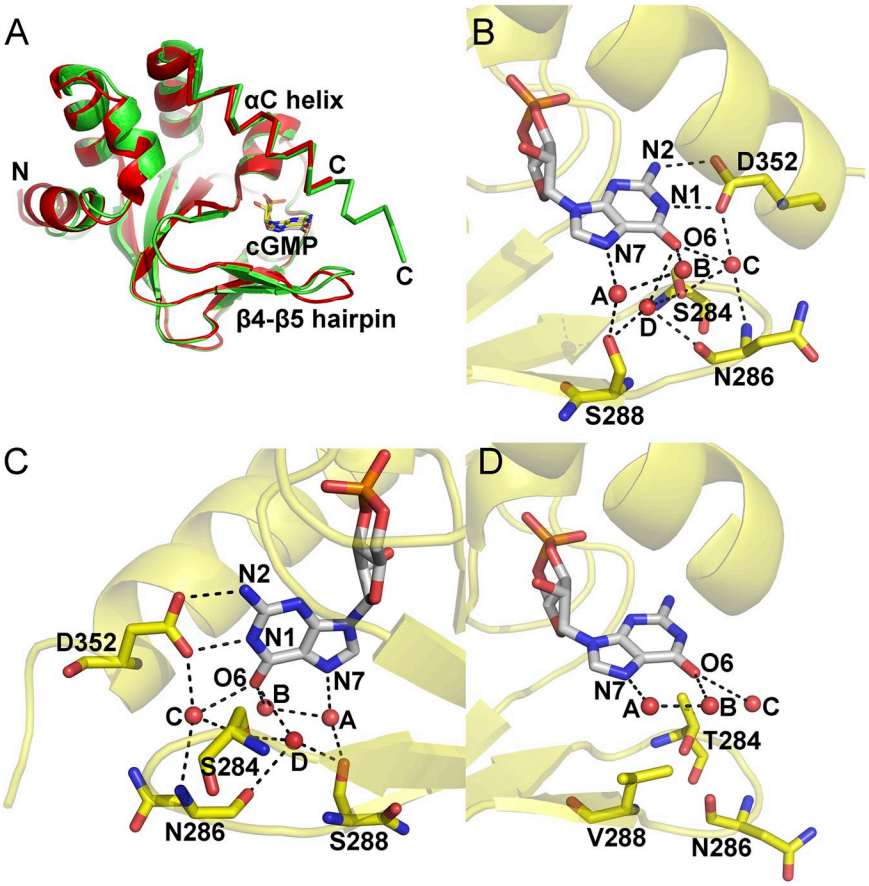

Figure 3. Structural characterization of the T284S/V288S/A352D MlotiK1 CNB domain mutant. (A) Superposition of triple mutant (green) and wild-type (red) CNB domain structures in complex with cGMP. Ligands are represented as stick. Some structural elements of the binding pocket are indicated. (B) Detail of the ligand-binding pocket of the triple mutant. cGMP is shown in white stick, with some of the residues in the pocket shown in yellow. Water molecules bound in the ligand-binding pocket are shown as red spheres. Dashed lines connect some of the atoms within hydrogen bond distance. The rest of the protein is shown in transparent cartoon. (C) As in B, but viewed from just below the β4–β5 hairpin. (D) View as in B of the ligand-binding pocket of one of the asymmetric unit protein molecules present in the cGMP-bound wild-type CNB domain crystals. Some of the residues in the hairpin and the three waters present in the binding pocket are shown.

Published June 30, 2014

There are, however, interesting differences in the binding pocket. First, the αC helix in the mutant, where A352D was introduced, is five to six residues longer and the domain structure ends at residue 354 or 355 (Fig. 3 A), depending on the asymmetric unit molecule considered. Second, the β4–β5 hairpin in the mutant, where the other two mutations were introduced, adopts a different conformation relative to the wild-type structure, closing further over the ligand (Fig. 3 A). Despite these differences, the nucleotides adopt the same *syn* conformation and are in similar positions.

A more detailed analysis of the triple mutant interactions between the protein and the nucleotide base shows that V282, M299, S308, and R348 interact with the ligand in the same way as in the wild-type structure. In one of the asymmetric unit mutant copies, the side-chain methyl groups of A309 and A351 are also within 4 Å of the base, but this is not observed in the other copy. More

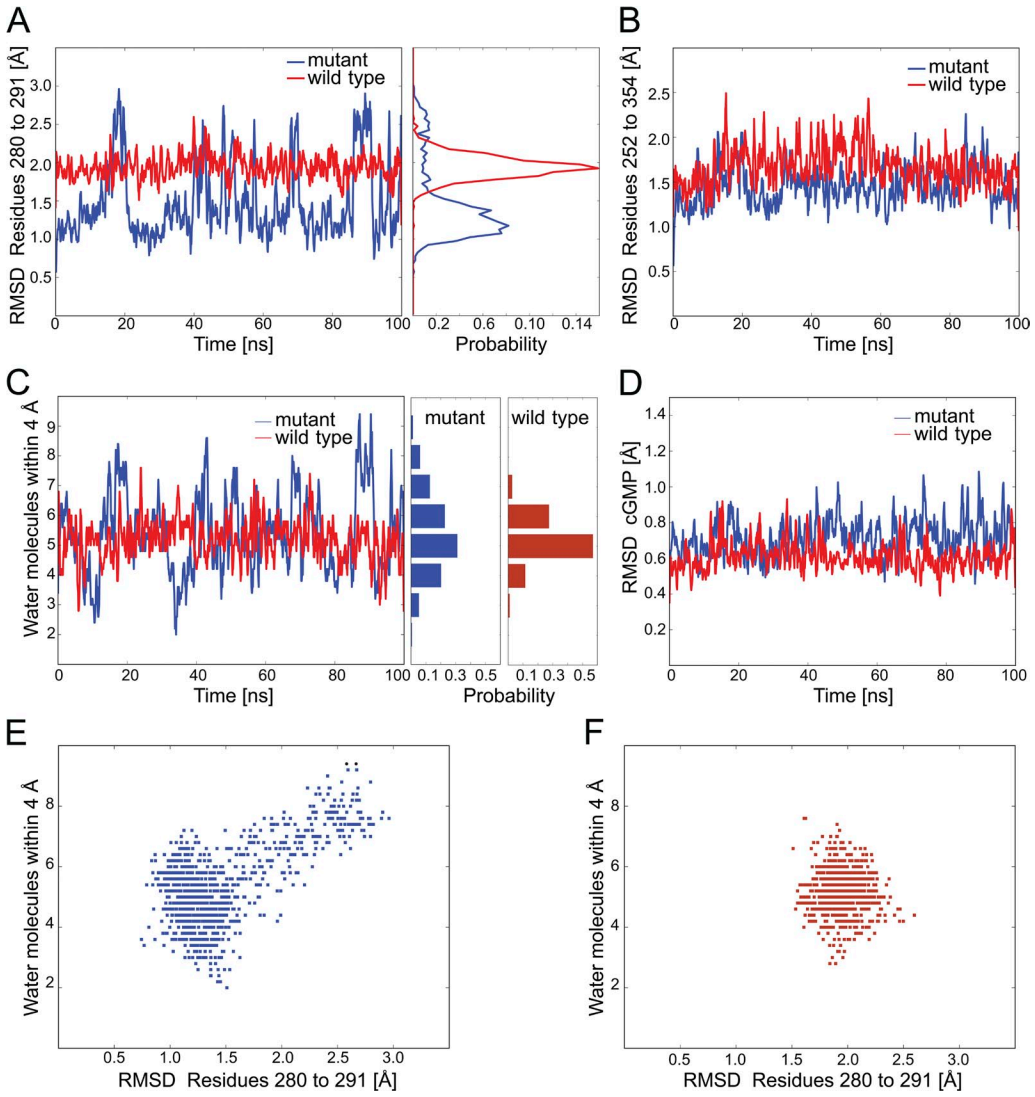

Figure 4. MD simulations of the MlotiK1 CNB domain. MD trajectories were sampled with a period of 10 ps. Data for the wild-type CNB domain and for the T284S/V288S/A352 mutant are shown, respectively, in red and in blue. (A) RMSD of the backbone atoms in the β4–β5 hairpin (residues 280–291). The probability histograms shown on the right side of the panel were calculated using a bin size of 0.05 Å. (B) RMSD of the backbone atoms of residues 252–354, corresponding to the whole CNB domain. In A and B, all of the MD snapshots were superimposed on the corresponding crystal structure, using the heavy atoms of cGMP as reference. (C) Number of water molecules closer than 4.0 Å from heavy atoms of the nucleotide base. At the beginning of the simulation, the structure contains six waters within 4.0 Å of the base. (D) RMSD of the heavy atoms of cGMP. All the MD snapshots were superimposed on the corresponding crystal structure, using the backbone atoms of residues 252–354 as reference. (E and F) Number of water molecules closer than 4.0 Å from heavy atoms of the nucleotide base as a function of the RMSD of the backbone atoms in the β4–β5 hairpin (residues 280–291), (E) in the mutant and (F) wild-type domains.

Published June 30, 2014

interesting are the differences in the structural roles of the three mutations (T284S, V288S, and A352D). The A352D side chain extends toward the nucleotide base, with the carboxylic group hydrogen bonding N1 and N2 of the guanine (Figs. 3, B and C, and S3) and anchoring the end of the αC helix to the body of the domain. This interaction mirrors a similar disposition seen in the I336D–HCN2 CNB domain structure (Flynn et al., 2007). In contrast, T284S and V288S are either beyond the 4-Å range for Van der Waals interactions with the nucleotide base or at the far end of this type of interaction, leading us to conclude that these residues do not establish close interactions with the nucleotide. Instead, T284S and V288S are involved in a hydrogen bond network with four water molecules present in the binding pocket (Fig. 3, B and C). Waters A and B are positioned along the rim of the guanine ring, whereas waters C and D are positioned between the β4–β5 hairpin and the nucleotide base. The B factors of the four waters and of the surrounding protein atoms are similar, indicating that these waters are stably bound in the crystal. This water network connects several residues in the binding pocket to each other and to the nucleotide base. Water A bridges V288S and N7 in the nucleotide base and is also within hydrogen-bonding distance of water B; water B also hydrogen bonds O6 in the nucleotide base. Water C is within hydrogen-bonding distance of the carboxylic group of A352D, of the hydroxyl in T284S, of O6 in the nucleotide, and of the main-chain amino group in N286 in the β4–β5 hairpin. Finally, water D is within hydrogen-bonding distance of O6 in the nucleotide base, of the hydroxyl groups in V288S and T284S, and of the carbonyl of N286. Analysis of the previously determined structures of the MlotiK1 CNB domain reveals that in one of the asymmetric unit protein copies of the cGMP-bound wild-type domain crystal structure (Fig. 3 D), there are water molecules in the binding pocket that are equivalent to waters A, B, and C. However, they do not form a hydrogen bond network in the ligand pocket, and they are not observed in the other protein copy.

Exploring the binding pocket interactions with MD simulations

To get a more complete view of the interactions between the ligand-binding pocket residues and the nucleotide, we performed MD simulations with the triple mutant and the wild-type CNB domain structures bound to cGMP.

Interestingly, a plot of β4–β5 hairpin backbone atom RMSD over the duration of the simulation revealed that the mutant structure hops repeatedly between two or three different conformations, corresponding to RMSDs of ∼1.1, ∼1.5, and 2.0–2.5 Å, whereas the wild-type structure oscillates around a more uniform average structure (Fig. 4 A). Further analysis reveals that, in the triple mutant simulations, there is a correlation between the number of waters and the different hairpin conformations (Fig. 4, A, C, and E) so that higher RMSD values correspond to a higher number of waters within 4 Å of the base. Thus, transition between the different conformations is accompanied by movement of water molecules

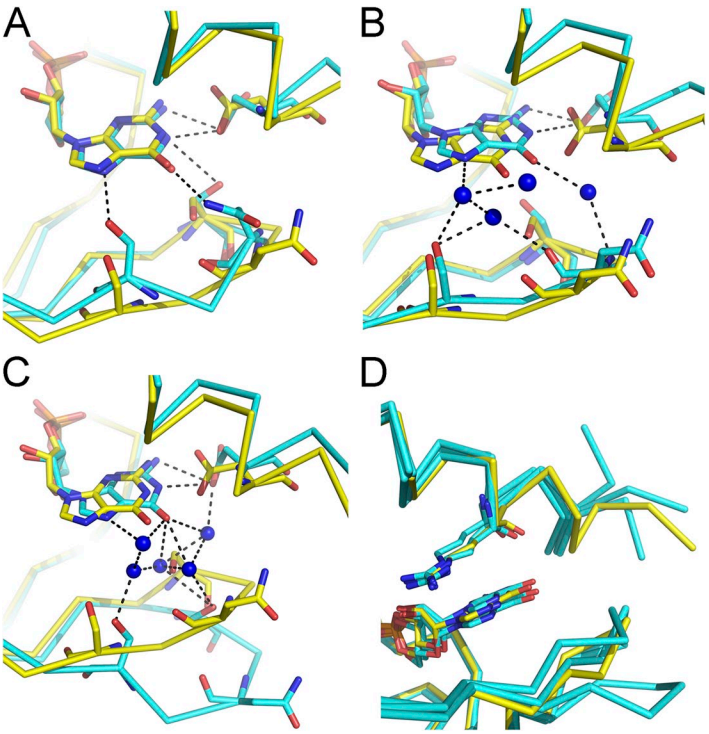

Figure 5. MD simulation conformational states. View of the superposed ligand-binding pockets from the triple mutant crystal structure (yellow stick) and from MD simulation snapshot models (cyan) in the (A) closed conformation, (B) semi-closed conformation, and (C) open conformation. Structures are shown as Cα traces, with ligands in yellow (crystal structure) or cyan (MD simulation models). Only waters that mediate protein–ligand interactions are shown (as blue spheres). Dashed lines connect some of the atoms within hydrogen bond distance. (D) Superposition of crystal structure and MD simulation snapshot structures in the different conformations. View of the ligand-binding pocket with cGMP and R348 shown as stick.

Published June 30, 2014

in and out of the nucleotide neighborhood. In contrast, a similar plot for the wild-type simulation shows a rapid fluctuation in the number of waters around the average value of five to six waters (Fig. 4 F).

Analysis of snapshot structures corresponding to the different conformations of the triple mutant revealed: a closed conformation in which the hairpin moves toward the base (Fig. 5 A), establishing closer interactions with the ligand base; a semi-closed conformation that strongly resembles the crystal structure (Fig. 5 B); and an open conformation where the hairpin moves away from the nucleotide base (Fig. 5 C). These conformations are associated with different numbers of water molecules in the binding pocket so that: the closed conformation has no or very few waters within hydrogen-bonding distance of the base; the semi-closed has approximately four waters within hydrogen-bonding distance of the base, just like the crystal structure; and the open conformation has a larger number of waters forming a network that connects the ligand and the protein. Importantly, the nucleotide and the αC helix remain stable throughout the simulation and in all of these conformations (Figs. 4 D and 5 D), indicating that the bound state of the domain is not affected by these conformational changes around the nucleotide, and that the ligand can be stabilized either by direct protein contacts or water-mediated contacts.

In addition, visual inspection of the triple mutant crystal lattice reveals that the β4–β5 hairpin is tightly packed against other protein molecules in the lattice. Therefore, it seems reasonable to conclude that during crystal formation there is a selection of one of the conformational states sampled by the ligand-binding pocket and that the MD simulation has uncovered the existence of other conformations.

The analysis of hydrogen bonds formed between the protein and the nucleotide base during the MD simulations shows that in the wild-type structure, there is an average of one hydrogen bond formed directly with protein atoms and one bond that is mediated by water (we did not consider interactions that might be mediated by more than one water molecule). In the triple mutant, the numbers are 2.5 for direct bonds and 1 for water mediated. A breakdown of these hydrogen bonds among the binding pocket residues is shown in Table 2. The direct hydrogen bond formed between S308 and N7 in the base is present both in the wild-type and mutant protein and is highly stable over the length of the simulations, agreeing well with the demonstrated importance of this residue for the stability of bound cGMP (Altenhofen et al., 1991; Flynn et al., 2007). The hydrogen bonds that are present in the mutant but not in the wild-type simulations are caused by A352D, which forms a long-lived interaction with the ligand through its carboxylic group, and V288S, which either forms a direct or a water-mediated hydrogen bond over a good fraction of the simulation time. The water-mediated interaction between V288S and the ligand is present in the crystal structure of the mutant (Fig. 3, B and C) as well as in the simulation semi-closed conformation (Fig. 5 B); the direct hydrogen bond involving this residue occurs in the simulation closed conformation, when the binding pocket loses water molecules and the hairpin approaches the nucleotide base (Fig. 5 A).

The analysis of the MD simulations suggests that there are two aspects that contribute favorably for the tighter binding of cGMP by the mutant. The detection in the triple mutant MD simulation of several conformations of the ligand-binding site, whereas in the wild-type domain only one conformation is observed, suggests that tighter binding of cGMP in the triple mutant involves a more favorable entropic component. In addition, several factors indicate that the tighter cGMP binding in

TABLE 2

Stability of hydrogen bonds formed between protein and ligand base during MD simulation

	Wild type		T284S/V288S/A352D	
Residue	Protein–cGMP h-bonds	Water-mediated h-bonds	Protein–cGMP h-bonds	Water-mediated h-bonds
284	2% (OG1)	23% (OG1)	—	10% (OG)
286	—	35% (ND2) +20% (N) +3% (O)	6% (ND2)	22% (O) +9% (N) +4% (ND2)
288	—	—	24% (OG)	35% (OG)
297	—	—	—	—
298	—	—	—	—
308	95% (OG)	3% (O)	93% (OG)	—
348	—	6% (NE) +2% (O)	—	2% (NE)
352	—	—	67% (OD2) +61%(OD1)	7% (OD1) +7% (OD2)

Percentages correspond to the fraction of time in the MD trajectory when a protein residue forms a hydrogen bond (h-bond) with the guanine group. The name of the protein atom participating to the h-bond is given in parentheses. Two atoms are considered part of an h-bond if donor and acceptor are closer than 3.5 Å and the donor–hydrogen–acceptor angle is below 35°.

Published June 30, 2014

the triple mutant is also the result of an increase in the polar chemical nature of the binding pocket: (a) all of the mutations introduced in the triple mutant have a strong polar chemical character, and (b) our analysis of both the crystal structure and MD simulation show that A352D and V288S are involved in polar interactions (direct or water mediated) with the nucleotide. An estimation of the polar energy contribution to the total energy of cGMP binding in the wild-type and mutant domains supports this proposal. A quantitative comparison of the estimated binding energies with experimental data is not possible because of the approximations applied; for example, the entropic contribution to the binding energy is not considered. Nevertheless, these approximations are not expected to affect greatly the main result of our energetic analyses (Table 3), which shows that the polar component of the binding energy is more favorable for cGMP binding in the mutant (−6.4 kcal/mol) than in the wild-type domain (−2.8 kcal/mol). In contrast, the apolar term is less favorable in the mutant than in the wild-type domain.

Impact of individual mutations in the triple mutant CNB domain

We also analyzed the role of the individual mutated residues on the stability of the mutant complex by measuring the ligand-binding properties of the single-point mutant domains (Table 1). The A352D single-point mutant has lower ligand selectivity than the wild-type domain (approximately three times preference for cAMP). This results from a decrease in cAMP affinity (K_d cAMP: 256 ± 29 nM) and an increase in cGMP affinity (K_d cGMP: 850 ± 121 nM). On the other hand, the V288S single-point mutant domain is almost nonselective (1.7× preference for cAMP) because of a large decrease in cAMP affinity (K_d cAMP: 1,205 ± 160 nM), with no effect on cGMP (K_d cGMP: 2,105 ± 128 nM). Similarly, the relatively neutral substitution of T284 for serine reduced cAMP affinity (K_d cAMP: 464 ± 58 nM) while having little effect on cGMP (K_d cGMP: 2,984 ± 379 nM), so that its overall selectivity decreased to an approximately six times cAMP preference.

The increased affinity for cGMP in the A352D mutant fits well with the close interaction between this residue and the ligand seen in the crystal and in the MD simulation. The almost neutral effect of T284S on cGMP binding also fits well with the structural and simulation data where no specific interactions are observed between this residue and cGMP. In contrast, the crystal structure and the MD simulations led us to expect that the V288S mutant would show tighter cGMP binding, but the affinity measurements in the V288S single mutant show no impact on cGMP binding. In addition, none of the single mutants alone causes the inversion in ligand selectivity, strongly suggesting that inversion in ligand selectivity is caused mainly by an effect that results from the combination of the three residue changes (T284S/V288S/A352D). To dissect the underlying details of this combination of mutations, we performed a mutant cycle energetic coupling analysis (Carter et al., 1984; Schreiber and Fersht, 1995; Ranganathan et al., 1996; Yifrach et al., 2009). More specifically, in a double mutant cycle analysis of ligand binding, a coupling energy above or below zero indicates that there is a difference in the energetic interaction of two side chains between the bound and unbound states.

After determining the affinity of the V288S/A352D double mutant for cAMP and cGMP (K_d cAMP: 547 ± 111 nM and K_d cGMP: 351 ± 95 nM [Table 1], corresponding to an ∼0.6× preference for cAMP), we calculated the coupling energies between these two residues. For cAMP binding, the coupling energy is −0.78 ± 0.18 kcal/mol, and for cGMP binding, it is −0.64 ± 0.20 kcal/mol. We also determined the coupling energies for the combination of T284S with V288S/A352D: 0.14 ± 0.19 kcal/mol for cAMP binding and −0.34 ± 0.29 kcal/mol for cGMP binding. The V288S/A352D plus T284S coupling energies are small and, within their associated error, close to zero, so we consider that they represent independent effects. In contrast, analysis of the mutant cycle for V288S and A352D (Fig. S4) shows that the impact of V288S in the absence or presence of A352D is different. V288S alone has no effect (0.12 ± 0.10 kcal/mol) in cGMP binding but has a stabilizing impact (−0.52 ± 0.18 kcal/mol) when combined with A352D. This stabilization fits nicely with the type of interactions observed in the crystal structure and MD simulations between this residue and the ligand. Additionally, it is worthwhile considering that in the triple mutant structure, these two residues are far from each other (∼8 Å) and, most likely, even further away in the unbound-state structures (Clayton et al., 2004; Altieri et al., 2008; Schünke et al., 2009, 2011); the coupling energies for this residue pair are therefore larger than the coupling energy values determined by Schreiber and Fersht (1995) for residue pairs separated by more than

TABLE 3

Binding energies estimated with MM/PBSA

CNB domain	E_{apolar}	E_{polar}	E_{tot}
	kcal/mol	*kcal/mol*	*kcal/mol*
Wild type	−49.1 ± 0.3	−2.8 ± 0.3	−51.9 ± 0.4
Mutant	−47.1 ± 0.4	−6.4 ± 0.3	−53.4 ± 0.4
ΔG(mutant)-ΔG(wild-type)	2.0 ± 0.7	−3.6 ± 0.6	−1.5 ± 0.8

Binding energies are reported as average values ± standard errors calculated over 100 samples (100-ns MD trajectories sampled with a period equal to 1 ns). The total binding energy (E_{tot}) is the sum of an apolar term (E_{apolar}; equal to the Van der Waals energy plus the apolar contribution to the solvation energy) and a polar term (E_{polar}; equal to the coulombic energy plus the polar contribution to the solvation energy).

Published June 30, 2014

7 Å (all <|0.5| kcal/mol) on the interface of the barstar–barnase protein complex. It is possible to envisage that a long-distance interaction between V288S and A352D could result from the stabilization of the water molecule network present in the binding pockets of the crystal and simulation structures. However, the V288S/A352D coupling energies are smaller than the |1| kcal/mol arbitrary barrier commonly used to define cooperative effects; therefore, we cautiously considered this residue combination as additive.

Exploring other residues in the binding pocket

In addition to the three mutations described above, we evaluated the impact of various other binding pocket mutations. We have summarized the results of this analysis in Table 1. Overall, this mutant screening shows that, although some of the tested single mutants greatly reduce the domain's preference for cAMP over cGMP, none of these single mutations (including those found to determine selectivity in other cyclic nucleotide–regulated channels) caused a reversal of selectivity, as defined by the ratio of the K_ds.

We have found specific effects that provide new insights into the general ligand-binding properties of CNB domains. The lack of a clear definition of which residues in the binding pocket favor cAMP binding explains in part our incomplete understanding of the molecular determinants of cyclic nucleotide binding in CNB domains. It has been shown in HCN2 channels that residues at the C-terminal end of the αC helix affect cAMP binding (Zhou and Siegelbaum, 2007), but these do not appear to interact directly with the nucleotide. We have now found that apolar residues (valine, leucine, isoleucine, and alanine) at position 288 of MlotiK1, in the β4–β5 hairpin and in the immediate neighborhood of the nucleotide base, favor cAMP binding. This conclusion results from finding that the presence of the apolar amino acids at this position maintains tight cAMP binding and cAMP preference over cGMP (Table 1), whereas the introduction of a serine (V288S) caused a large decrease in the affinity for cAMP and made the mutant almost nonselective (Table 1).

In addition, we have confirmed the importance of a negatively charged amino acid at the end of the αC helix (Varnum et al., 1995; Flynn et al., 2007) at position 352, for the increased stability of the cGMP complex (Table 1). Also, we showed that a serine, at this same position (A352S), increases cGMP affinity (K_d cGMP: 727 ± 170 nM) while not altering cAMP affinity (K_d cGMP: 174 ± 23 nM).

We also looked at substitutions in R348 (Table 1), a residue that has an important role in the closure of the αC helix over the ligand and therefore on the stabilization of the bound state of CNG (Puljung and Zagotta, 2013), HCN (Zhou and Siegelbaum, 2007), and MlotiK1 channels (Clayton et al., 2004; Altieri et al., 2008; Mari et al., 2011) (Fig. S1). In the MlotiK1 channel, this is illustrated by several observations within the CNB domain: the interactions established by the arginine in the nucleotide-bound domain structures (Clayton et al., 2004; Altieri et al., 2008; Schünke et al., 2009); the greatly reduced cAMP affinity of the R348A mutant domain (Cukkemane et al., 2007; Peuker et al., 2013); and in the channel, by the high $K_{1/2}$ for the nucleotide dependence of activation in the R348A mutant channel and by its lower flux activity at saturating concentrations of ligand (Mari et al., 2011).

We first confirmed that R348A is almost nonselective (K_d cAMP: 25 ± 3.2 µM; K_d cGMP: 39 ± 2.5 µM) and then tested other side chains at this position. In particular, we wondered whether residues with long polar side chains could replace the arginine by retaining the interactions with the nucleotide base and also the hydrogen bonding with residues in the binding pocket. Strikingly, mutations R348N, R348Q, and R348K have basically the same ligand-binding properties as R348A, with affinities for cAMP and cGMP that vary between 16 and 46 µM and are almost nonselective (1.4–1.8× for cAMP). Because of the low affinity for the fluorescent analogue displayed by all mutations of R348, we used a slightly different titration procedure (see Materials and methods and Table 1). We also evaluated if electronic delocalization in the side chain was a determining factor at this position by measuring ligand-binding affinities for the mutant R348Y; however, results are very similar to R348A (K_d cAMP: 24 ± 2.2 µM; K_d cGMP: 33 ± 4.8 µM). Collectively, these results show that R348, in the αC helix, is a major determinant of nucleotide affinity (both cAMP and cGMP), as it was the only residue where mutations caused K_d changes >10-fold and resulted in large changes in ligand selectivity. Our results mirror previous findings in other cyclic nucleotide–regulated channels (Craven and Zagotta, 2006; Flynn et al., 2007; Zhou and Siegelbaum, 2007; Puljung and Zagotta, 2013). Collectively, these results support the general importance of the αC helix arginine for the stabilization of the "bound-activated state" through closure of the αC lid over the nucleotide and show that the physical–chemical properties of the arginine side chain are essential for this role.

DISCUSSION

Our analysis in the MlotiK1, together with a study by Nimigean and Pagel (2007), confirmed the importance of specific binding pocket residues for cGMP binding (Table 1), a serine/threonine at the end of the PBC sequence, and an aspartate at the end of the αC helix. We also established that apolar residues on the β4–β5 hairpin favor cAMP binding.

In certain cyclic nucleotide–regulated proteins, the presence of one of the residues discussed above is sufficient

Published June 30, 2014

for determining preference for cGMP over cAMP. However, in the MlotiK1 CNB domain, and in many other cyclic nucleotide–regulated proteins, this is not true (Cukkemane et al., 2011), and it is clear that other factors (other residues and/or structural features) also play a role in ligand selectivity. We inverted ligand selectivity in the MlotiK1 channel with a combination of mutations at T284S, V288S, and A352D. The x-ray structure of our triple mutant shows that A352D establishes close contacts with the guanine group, whereas the other two residues are involved with a network of four water molecules that connect the protein and the ligand. Surprisingly, an MD simulation reveals that the conformation seen in the crystal is not unique; in the simulation, the crystal conformation (or semi-closed conformation) appears to be in equilibrium with two other conformations: a closed conformation where the β4–β5 hairpin is positioned closer to the nucleotide base and V288S forms direct interactions with the guanine group, and an open conformation where the hairpin has moved away from the ligand and contacts between the protein and the ligand involve a network of many waters. Importantly, all of these different conformations appear to correspond to a bound-activated state of the domain, as the nucleotide position and the position of the αC helix do not vary greatly over the length of the simulation. In contrast, the MD simulation of the cGMP-bound wild-type domain shows only one conformation.

The "structural freedom" of the triple mutant ligand-binding pocket observed in the MD simulation, involving multiple conformations of the β4–β5 hairpin and movement of solvent molecules in and out of the pocket, strongly suggests that the increased stability of the cGMP complex in this mutant is partly caused by an increase in the entropy of the bound state relative to the wild-type domain. In addition, our mutagenesis analysis together with the crystal structure and MD simulation also strongly indicates that there is a combined effect of the three mutations (T284S/V288S/A352D) to create a polar environment around the nucleotide base involving interactions of water molecules with the protein. This conclusion is based on several factors: the increased polar chemical character of all the substitutions; the larger number of hydrogen bonds established between the protein and the ligand in the simulation closed and semi-closed conformations relative to the wild-type domain; the larger number of water molecules that solvate the ligand in the simulation open conformation; and the calculated contribution of the polar energy to the total binding energy of the ligand. Importantly, the significance of the polar environment for defining cGMP preference in our mutant domain is supported by theoretical calculations that show that the cGMP hydration energy is greater than for cAMP (Zhou and Siegelbaum, 2008). This theoretical finding suggests that preference for cGMP binding in a CNB domain can be generally achieved through a binding pocket that either compensates for ligand dehydration or allows many of the solvation waters to be retained in the bound state. These are exactly the features that we have found in our analysis of the MlotiK1 triple mutant.

In this context, it is also interesting to analyze the recently published structure of the cGMP-bound CNB β domain from the cGMP-dependent protein kinase I (Protein Data Bank accession no. 4KU7) (Huang et al., 2014), a domain that is ∼250 times more selective for cGMP than cAMP (Figs. S1 and S5). Its binding pocket includes an arginine at a position that is equivalent to residue 288 in MlotiK1; importantly, it was shown that mutation of this residue to alanine strongly affects the selectivity properties of the domain. In the structure, the arginine hydrogen bonds N7 and O6 in the guanine base, resembling the interactions established between the waters A and B and the base in our triple mutant structure (Fig. S5, A and B). In addition, the ligand base is highly exposed to the bulk solvent (Fig. S5, C and D) because the αC helix is very short and the tip of the β4–β5 hairpin is disordered. Collectively, this analysis shows that the ligand-binding pocket of this strongly cGMP-selective CNB domain shares some of the polar environment characteristics described above in the MlotiK1 triple mutant domain.

Our conclusion that the polar character and the structural freedom of the ligand-binding pocket in the triple mutant are determining factors for cGMP preference also explains the difficulty in establishing rules for determining the selectivity properties of a CNB domain just from an amino acid sequence. These prediction rules cannot just consider the possible direct interactions between side chains and the nucleotide chemical groups. They have to consider that there are multiple mechanisms for establishing selectivity in a CNB domain, mechanisms that include more complex effects such as the stabilization of water molecules in the ligand-binding pocket or differences in the entropy of this pocket.

We thank Andras Szollosi, Nuno Mateus, Iva Fernandes, Ricardo S. Vieira-Pires, Enrique de la Cruz, Wenxiang Cao, and Carol Harley for their help. We also thank ESRF for access to ID14-4 through the Portuguese BAG.

We thank the Fundação para a Ciência e a Tecnologia for a PhD fellowship (SFRH/BD/60274/2009 to J. Pessoa) and a post-doctoral fellowship (SFRH/BPD/77040/2011 to F. Fonseca). This work was funded by FEDER Funds through the Operational Competitiveness Program– COMPETE and by national funds through FCT–Fundação para a Ciência e a Tecnologia under the project FCOMP-01-0124-FEDER-028185 (PTDC/BBB-BQB/1418/2012 awarded to J.H. Morais-Cabral). CINECA is acknowledged for providing high performance computing resources through Award N. HP10BX4MV5.

The authors declare no competing financial interests.

Sharona E. Gordon served as editor.

Submitted: 5 December 2013
Accepted: 10 June 2014

Published June 30, 2014

REFERENCES

Afonine, P.V., R.W. Grosse-Kunstleve, N. Echols, J.J. Headd, N.W. Moriarty, M. Mustyakimov, T.C. Terwilliger, A. Urzhumtsev, P.H. Zwart, and P.D. Adams. 2012. Towards automated crystallographic structure refinement with *phenix.refine*. *Acta Crystallogr. D Biol. Crystallogr.* 68:352–367. http://dx.doi.org/10.1107/S0907444912001308

Altenhofen, W., J. Ludwig, E. Eismann, W. Kraus, W. Bönigk, and U.B. Kaupp. 1991. Control of ligand specificity in cyclic nucleotide-gated channels from rod photoreceptors and olfactory epithelium. *Proc. Natl. Acad. Sci. USA.* 88:9868–9872. http://dx.doi.org/10.1073/pnas.88.21.9868

Altieri, S.L., G.M. Clayton, W.R. Silverman, A.O. Olivares, E.M. De la Cruz, L.R. Thomas, and J.H. Morais-Cabral. 2008. Structural and energetic analysis of activation by a cyclic nucleotide binding domain. *J. Mol. Biol.* 381:655–669. http://dx.doi.org/10.1016/j.jmb.2008.06.011

Baker, N.A., D. Sept, S. Joseph, M.J. Holst, and J.A. McCammon. 2001. Electrostatics of nanosystems: Application to microtubules and the ribosome. *Proc. Natl. Acad. Sci. USA.* 98:10037–10041. http://dx.doi.org/10.1073/pnas.181342398

Carter, P.J., G. Winter, A.J. Wilkinson, and A.R. Fersht. 1984. The use of double mutants to detect structural changes in the active site of the tyrosyl-tRNA synthetase (*Bacillus stearothermophilus*). *Cell.* 38:835–840. http://dx.doi.org/10.1016/0092-8674(84)90278-2

Chiu, P.L., M.D. Pagel, J. Evans, H.T. Chou, X. Zeng, B. Gipson, H. Stahlberg, and C.M. Nimigean. 2007. The structure of the prokaryotic cyclic nucleotide-modulated potassium channel MloK1 at 16 Å resolution. *Structure.* 15:1053–1064. http://dx.doi.org/10.1016/j.str.2007.06.020

Clayton, G.M., W.R. Silverman, L. Heginbotham, and J.H. Morais-Cabral. 2004. Structural basis of ligand activation in a cyclic nucleotide regulated potassium channel. *Cell.* 119:615–627. http://dx.doi.org/10.1016/j.cell.2004.10.030

Clayton, G.M., S. Altieri, L. Heginbotham, V.M. Unger, and J.H. Morais-Cabral. 2008. Structure of the transmembrane regions of a bacterial cyclic nucleotide-regulated channel. *Proc. Natl. Acad. Sci. USA.* 105:1511–1515. http://dx.doi.org/10.1073/pnas.0711533105

Craven, K.B., and W.N. Zagotta. 2006. CNG and HCN channels: Two peas, one pod. *Annu. Rev. Physiol.* 68:375–401. http://dx.doi.org/10.1146/annurev.physiol.68.040104.134728

Cukkemane, A., B. Grüter, K. Novak, T. Gensch, W. Bönigk, T. Gerharz, U.B. Kaupp, and R. Seifert. 2007. Subunits act independently in a cyclic nucleotide-activated K^+ channel. *EMBO Rep.* 8:749–755. http://dx.doi.org/10.1038/sj.embor.7401025

Cukkemane, A., R. Seifert, and U.B. Kaupp. 2011. Cooperative and uncooperative cyclic-nucleotide-gated ion channels. *Trends Biochem. Sci.* 36:55–64. http://dx.doi.org/10.1016/j.tibs.2010.07.004

Emsley, P., B. Lohkamp, W.G. Scott, and K. Cowtan. 2010. Features and development of Coot. *Acta Crystallogr. D Biol. Crystallogr.* 66:486–501. http://dx.doi.org/10.1107/S0907444910007493

Essmann, U., L. Perera, M.L. Berkowitz, T. Darden, H. Lee, and L.G. Pedersen. 1995. A smooth particle mesh Ewald method. *J. Chem. Phys.* 103:8577–8593. http://dx.doi.org/10.1063/1.470117

Evans, P. 2006. Scaling and assessment of data quality. *Acta Crystallogr. D Biol. Crystallogr.* 62:72–82. http://dx.doi.org/10.1107/S0907444905036693

Feller, S.E., Y.H. Zhang, R.W. Pastor, and B.R. Brooks. 1995. Constant pressure molecular dynamics simulation: The Langevin piston method. *J. Chem. Phys.* 103:4613–4621. http://dx.doi.org/10.1063/1.470648

Flynn, G.E., K.D. Black, L.D. Islas, B. Sankaran, and W.N. Zagotta. 2007. Structure and rearrangements in the carboxy-terminal region of SpIH channels. *Structure.* 15:671–682. http://dx.doi.org/10.1016/j.str.2007.04.008

Furini, S., P. Barbini, and C. Domene. 2013. DNA-recognition process described by MD simulations of the lactose repressor protein on a specific and a non-specific DNA sequence. *Nucleic Acids Res.* 41:3963–3972. http://dx.doi.org/10.1093/nar/gkt099

Huang, G.Y., J.J. Kim, A.S. Reger, R. Lorenz, E.W. Moon, C. Zhao, D.E. Casteel, D. Bertinetti, B. Vanschouwen, R. Selvaratnam, et al. 2014. Structural basis for cyclic-nucleotide selectivity and cGMP-selective activation of PKG I. *Structure.* 22:116–124. http://dx.doi.org/10.1016/j.str.2013.09.021

Jorgensen, W.L., J. Chandrasekhar, J.D. Madura, R.W. Impey, and M.L. Klein. 1983. Comparison of simple potential functions for simulating liquid water. *J. Chem. Phys.* 79:926–935. http://dx.doi.org/10.1063/1.445869

Kabsch, W. 2010. XDS. *Acta Crystallogr. D Biol. Crystallogr.* 66:125–132. http://dx.doi.org/10.1107/S0907444909047337

MacKerell, A.D., D. Bashford, M. Bellott, R.L. Dunbrack, J.D. Evanseck, M.J. Field, S. Fischer, J. Gao, H. Guo, S. Ha, et al. 1998. All-atom empirical potential for molecular modeling and dynamics studies of proteins. *J. Phys. Chem. B.* 102:3586–3616. http://dx.doi.org/10.1021/jp973084f

Mari, S.A., J. Pessoa, S. Altieri, U. Hensen, L. Thomas, J.H. Morais-Cabral, and D.J. Müller. 2011. Gating of the MlotiK1 potassium channel involves large rearrangements of the cyclic nucleotide-binding domains. *Proc. Natl. Acad. Sci. USA.* 108:20802–20807. http://dx.doi.org/10.1073/pnas.1111149108

Martyna, G.J., D.J. Tobias, and M.L. Klein. 1994. Constant pressure molecular dynamics algorithms. *J. Chem. Phys.* 101:4177–4189. http://dx.doi.org/10.1063/1.467468

McCoy, A.J., R.W. Grosse-Kunstleve, P.D. Adams, M.D. Winn, L.C. Storoni, and R.J. Read. 2007. Phaser crystallographic software. *J. Appl. Cryst.* 40:658–674. http://dx.doi.org/10.1107/S0021889807021206

Miyamoto, S., and P.A. Kollman. 1992. Settle: An analytical version of the SHAKE and RATTLE algorithm for rigid water molecules. *J. Comput. Chem.* 13:952–962. http://dx.doi.org/10.1002/jcc.540130805

Nimigean, C.M. 2006. A radioactive uptake assay to measure ion transport across ion channel-containing liposomes. *Nat. Protoc.* 1:1207–1212. http://dx.doi.org/10.1038/nprot.2006.166

Nimigean, C.M., and M.D. Pagel. 2007. Ligand binding and activation in a prokaryotic cyclic nucleotide-modulated channel. *J. Mol. Biol.* 371:1325–1337. http://dx.doi.org/10.1016/j.jmb.2007.06.030

Nimigean, C.M., T. Shane, and C. Miller. 2004. A cyclic nucleotide modulated prokaryotic K^+ channel. *J. Gen. Physiol.* 124:203–210. http://dx.doi.org/10.1085/jgp.200409133

Peuker, S., A. Cukkemane, M. Held, F. Noé, U.B. Kaupp, and R. Seifert. 2013. Kinetics of ligand-receptor interaction reveals an induced-fit mode of binding in a cyclic nucleotide-activated protein. *Biophys. J.* 104:63–74. http://dx.doi.org/10.1016/j.bpj.2012.11.3816

Phillips, J.C., R. Braun, W. Wang, J. Gumbart, E. Tajkhorshid, E. Villa, C. Chipot, R.D. Skeel, L. Kalé, and K. Schulten. 2005. Scalable molecular dynamics with NAMD. *J. Comput. Chem.* 26:1781–1802. http://dx.doi.org/10.1002/jcc.20289

Pifferi, S., A. Menini, and T. Kurahashi. 2010. Signal transduction in vertebrate olfactory cilia. *In* The Neurobiology of Olfaction. CRC Press, Boca Raton, FL. 203–224.

Puljung, M.C., and W.N. Zagotta. 2013. A secondary structural transition in the C-helix promotes gating of cyclic nucleotide-regulated ion channels. *J. Biol. Chem.* 288:12944–12956. http://dx.doi.org/10.1074/jbc.M113.464123

Ranganathan, R., J.H. Lewis, and R. MacKinnon. 1996. Spatial localization of the K^+ channel selectivity filter by mutant cycle-based structure analysis. *Neuron.* 16:131–139. http://dx.doi.org/10.1016/S0896-6273(00)80030-6

Published June 30, 2014

Rehmann, H., A. Wittinghofer, and J.L. Bos. 2007. Capturing cyclic nucleotides in action: snapshots from crystallographic studies. *Nat. Rev. Mol. Cell Biol.* 8:63–73. http://dx.doi.org/10.1038/nrm2082

Schreiber, G., and A.R. Fersht. 1995. Energetics of protein-protein interactions: Analysis of the Barnase-Barstar interface by single mutations and double mutant cycles. *J. Mol. Biol.* 248:478–486. http://dx.doi.org/10.1016/S0022-2836(95)80064-6

Schünke, S., M. Stoldt, K. Novak, U.B. Kaupp, and D. Willbold. 2009. Solution structure of the *Mesorhizobium loti* K1 channel cyclic nucleotide-binding domain in complex with cAMP. *EMBO Rep.* 10:729–735. http://dx.doi.org/10.1038/embor.2009.68

Schünke, S., M. Stoldt, J. Lecher, U.B. Kaupp, and D. Willbold. 2011. Structural insights into conformational changes of a cyclic nucleotide-binding domain in solution from *Mesorhizobium loti* K1 channel. *Proc. Natl. Acad. Sci. USA.* 108:6121–6126. http://dx.doi.org/10.1073/pnas.1015890108

Varnum, M.D., K.D. Black, and W.N. Zagotta. 1995. Molecular mechanism for ligand discrimination of cyclic nucleotide-gated channels. *Neuron.* 15:619–625. http://dx.doi.org/10.1016/0896-6273(95)90150-7

Yifrach, O., N. Zandany, and T. Shem-Ad. 2009. Examining cooperative gating phenomena in voltage-dependent potassium channels: Taking the energetic approach. *Methods Enzymol.* 466:179–209. http://dx.doi.org/10.1016/S0076-6879(09)66008-0

Zhang, X., and R.H. Cote. 2005. cGMP signaling in vertebrate retinal photoreceptor cells. *Front. Biosci.* 10:1191–1204. http://dx.doi.org/10.2741/1612

Zhou, L., and S.A. Siegelbaum. 2007. Gating of HCN channels by cyclic nucleotides: Residue contacts that underlie ligand binding, selectivity, and efficacy. *Structure.* 15:655–670. http://dx.doi.org/10.1016/j.str.2007.04.012

Zhou, L., and S.A. Siegelbaum. 2008. Pathway and endpoint free energy calculations for cyclic nucleotide binding to HCN channels. *Biophys. J.* 94:L90–L92. http://dx.doi.org/10.1529/biophysj.108.130872

Pessoa et al., http://www.jgp.org/cgi/content/full/jgp.201311145/DC1

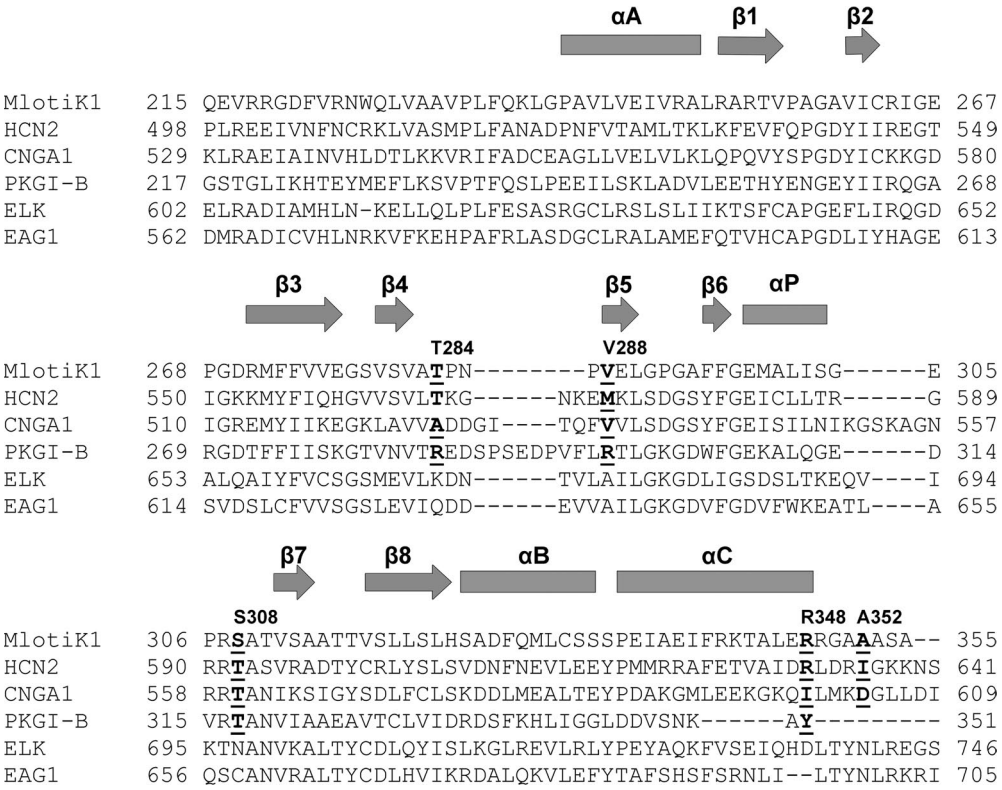

Figure S1. Sequence alignment of CNB domains from the MlotiK1 (UniProt accession no. Q98GN8), HCN2 (RefSeq accession no. NP_032252), and CNGA-1 channels (UniProt accession no. Q00194); CNB β domain from the cGMP-dependent kinase I (UniProt accession no. Q13976); and CNB homology domains from the ELK (RefSeq accession no. XP_001919436) and EAG1 (RefSeq accession no. NP_034730) channels. Secondary structure elements of MlotiK1CNB domain are shown as arrows (β strand) or rectangles (α helix). Residues that are discussed in the main text are shown in bold.

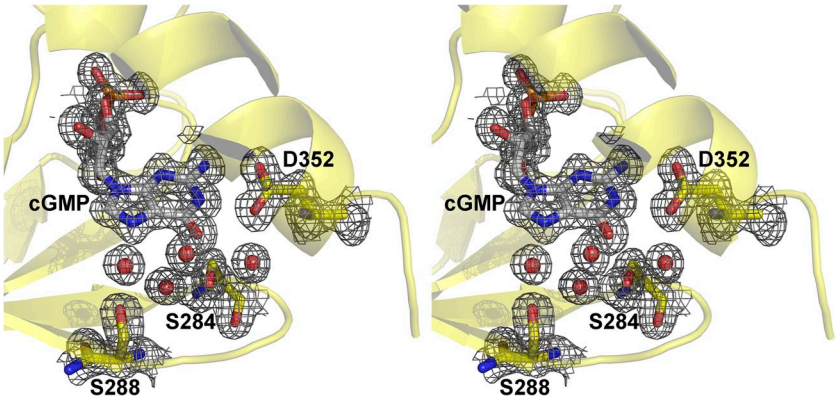

Figure S2. Stereo view of the 2Fo-Fc electron density map at 1.25-Å resolution covering the binding pocket of the T284S/V288S/A352D MlotiK1 CNB domain. cGMP and side chains of S288, D352, and S384 are represented as stick. Water molecules A–D are represented in red spheres. Electron density around these elements is represented by a gray mesh.

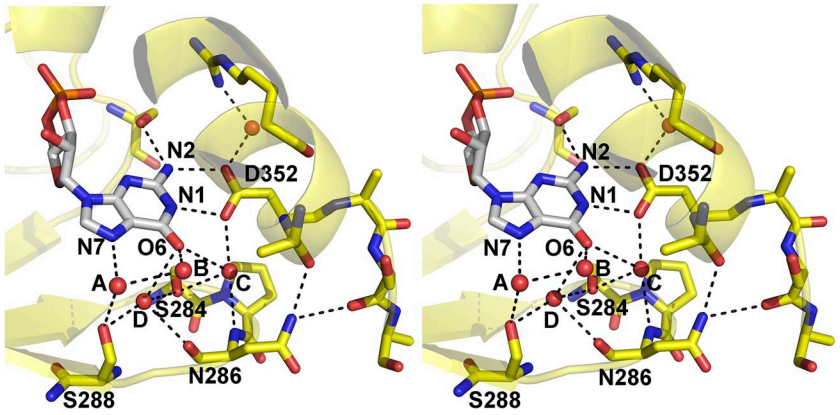

Figure S3. Stereo view of the ligand-binding pocket in the triple mutant. Water molecules are represented by red spheres, and the ligand (in white) and some residues (in yellow) are represented as stick. Residues and atoms discussed in the main text are labeled. The hydrogen bond network is represented by dashed lines.

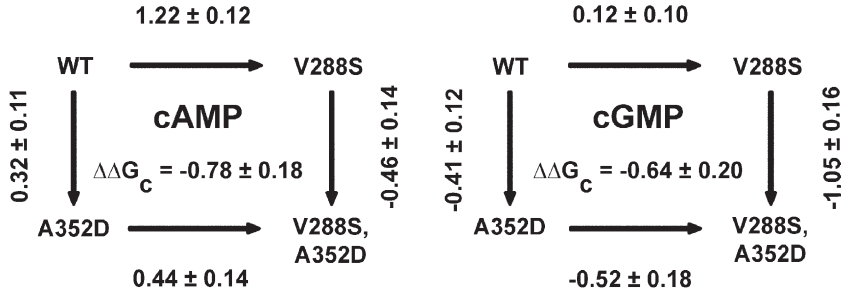

Figure S4. Mutant cycle energetic analysis. Mutant cycle of the V288S and A352D combination for cAMP (left) and cGMP binding (right). Corners correspond to wild-type, single, and double mutant CNB domain. Changes in ligand-binding energy (in kcal/mol) between different protein forms are indicated along the arrows connecting the corners. Coupling energy (ΔΔGc; in kcal/mol) is shown at the center of each panel.

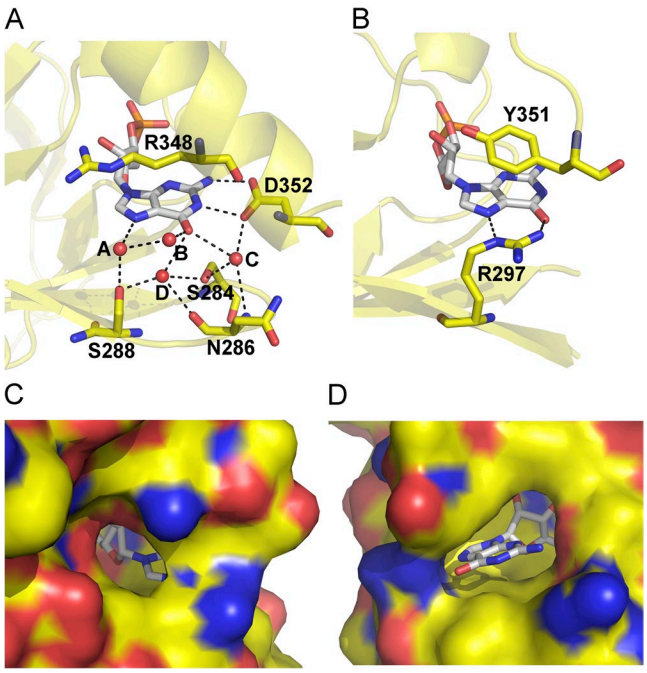

Figure S5. The CNB β domain from the cGMP-dependent protein kinase I. Identical views of the ligand-binding pocket in (A) the triple mutant domain from the MlotiK1 channel and in (B) the CNB β domain from the cGMP-dependent protein kinase I (Protein Data Bank accession no. 4KU7). Waters and some of the residues surrounding the nucleotide are labeled and shown as spheres and sticks, respectively. (C and D) Two views of the ligand-binding pocket in the CNB β domain from the cGMP-dependent protein kinase I, with the protein shown as a solvent-accessible surface. The figure shows that in this domain, the ligand is very exposed to the bulk solvent through two large water-accessible tunnels.

Table S1
Statistics of crystallographic data and refinement

Parameter	Value
Data collection	
Space group	P 2_1 2_1 2_1
Cell dimensions a, b, c (Å)	a = 60.05, b = 61.57, c = 67.84
Cell angles α, β, γ (°)	α, β, γ = 90.00
Resolution (Å)	42.99–1.22 (1.29–1.22)
R_{merge}	0.033 (0.646)
Total reflections	260,877 (33,195)
Unique reflections	74,662 (10,447)
$I/\sigma I$	20.9 (1.8)
Completeness (%)	99.0 (98.5)
Multiplicity	3.5 (3.2)
Refinement:	
Resolution (Å)	42.99–1.25 (1.27–1.25)
No. reflections	66,278 (3,514)
R_{work} / R_{free}	13.7/17.2
Number of atoms:	
Protein	4,402
Ligands	74
Solvent	355
Average B factor (all atoms) (Å^2)	18.0
RMSDs:	
Bond lengths (Å)	0.013
Bond angles (°)	1.56

Values in parentheses refer to the highest resolution shell.